Generalized Graph-Based Fusion of Hyperspectral and LiDAR Data Using Morphological Features

Wenzhi Liao, *Member, IEEE,* Aleksandra Pižurica, *Member, IEEE,* Rik Bellens, Sidharta Gautama, Wilfried Philips, *Senior Member, IEEE,*

***Abstract*—Nowadays, we have diverse sensor technologies and image processing algorithms that allow to measure different aspects of objects on the earth (spectral characteristics in hyperspectral (HS) images, height in LiDAR data, geometry in image processing technologies like morphological profiles (MPs)). It is clear that no single technology can be sufficient for a reliable classification, but combining many of them can lead to problems like the curse of dimensionality, excessive computation time and so on. Applying feature reduction techniques on all the features together is not a good either, because it does not take into account the differences in structure of the feature spaces. Decision fusion on the other hand has difficulties with modeling correlations between the different data sources. In this paper, we propose a *generalized* graph-based fusion method to couple dimension reduction and feature fusion of the spectral information (of original HS image) and MPs (built on both HS and LiDAR data). In the proposed method, the edges of the fusion graph are weighted by the distance between the stacked feature points. This yields a clear improvement over an older approach with binary edges in the fusion graph. Experimental results on real HS image and LiDAR data demonstrate effectiveness of the proposed method both visually and quantitatively.**

***Index Terms*—Data fusion, remote sensing, hyperspectral image, LiDAR data, graph-based**

I. Introduction

RECENT advances in the remote sensing technology of have led to an increased availability of multi-sensor data from the same area. In particular, hyperspectral (HS) images provide a detailed description of the spectral signatures of ground covers, whereas LiDAR data gives detailed information about the height of the same surveyed area. The HS data, once combined with LiDAR data, can provide a more comprehensive interpretation of objects on the ground. Many techniques have been developed for fusion of HS and LiDAR data in a classification task [1]–[6]. Simental *et al*. [1] explored the joint use of hyperspectral and LiDAR data for the separation of vegetation classes, underlining that LiDAR can be very useful in the separation of shrubs from trees. Lemp and Weidner [2] exploit HS and LiDAR data for the classification of urban areas, using LiDAR for the segmentation of the scene, and then HS data for the classification of the resulting regions. Koetz *et al*. [3] classified fuel composition from fused LiDAR and HS bands using support vector machines (SVM), and showed that the classification accuracies after fusion were higher than those based on either sensor alone. Multiple feature fusion using decision fusion and manifold learning were proposed for classification of HS remote sensing imagery in [7], [8]. Huang *et al*. [4] compared vector-stacking, re-classification and post-processing for information fusion of aerial images and LiDAR data in urban areas. The joint use of HS and LiDAR remote sensing data for the classification of complex forest areas was investigated in [5]. They proposed a novel classification system, based on different possible classifiers that were able to properly integrate multi-sensor information. Recently, Pedergnana *et al*. [6] applied morphological attribute profiles (EAPs) [9] to both HS and LiDAR data for a classification task. Their method jointly considered the features extracted by EAPs computed on both HS and LiDAR data, and fused spectral, spatial and elevation information in a stacked architecture.

Despite the simplicity of such feature fusion methods (that simply concatenate several kinds of feature sources), the systems do not always perform better (and can even perform worse) than using single feature source. Dalla Mura *et al*. [10] showed examples where the classification accuracies by stacking different morphological attributes were even lower than by using only single morphological attribute. This is because the information contained in different feature sources is not well represented or measured. Furthermore, the resulting data by stacking several kinds of feature sources may contain redundant information. Last, but not least, the increase in the dimensionality of the stacked features, as well as the limited number of labeled samples in many real applications may pose the problem of the curse of dimensionality and, as a consequence, result in the risk of overfitting the training data.

An older version of our graph-based data fusion method with binary edges of the fusion graph won the "Best Paper Challenge" award of 2013 IEEE Data Fusion Contest [11]. In this paper, we propose a *generalized* graph-based fusion of HS and LiDAR (GGF). An important difference with [11] is that the proposed fusion graph does not simply set the edges of fusion graph to 0 (disconnected) or 1 (connected), but employs *weighted* edges (with weights corresponding to the distance between the stacked feature points). This way we build a more general, weighted fusion graph where the actual differences and similarities in spectral, spatial and elevation characteristics of the feature points are better modeled. The proposed fusion graph is hence more general and more powerful than the

This work was financially supported by the SBO-IWT project Chameleon: Domain-specific Hyperspectral Imaging Systems for Relevant Industrial Applications.

Wenzhi Liao, Rik Bellens, Aleksandra Pižurica, Sidharta Gautama and Wilfried Philips are with the Department of Telecommunications and Information Processing, Ghent University - iMinds - Image Processing and Interpretation, Sint-Pietersnieuwstrat 41, 9000 Ghent, Belgium (email: {Wenzhi.Liao, Rik.Bellens, Aleksandra.Pizurica, Sidharta.Gautama, Wilfried.Philips}@telin.ugent.be).

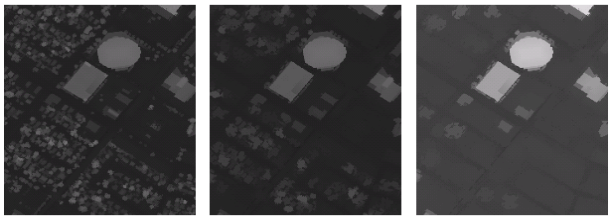

Fig. 1: Openings on a part of LiDAR data with disk-shaped SEs of increasing radius size (1, 3 and 5).

binary one. The organization of this letter is as follows. Section II provides a brief review of morphological features. In Section III, we present the proposed graph-based feature fusion method. The experimental results on real urban hyperspectral images are presented and discussed in Section IV. Finally, the conclusions of the paper are drawn in Section V.

II. Morphological features

Morphological features are generated by either applying morphological openings or closings by reconstruction on the image, using a structural element (SE) of predefined size and shape. For example, the morphological profile (MP) with disk SE carries information about the minimum size of objects, whereas directional MP indicates of the maximum size of objects [12]–[14]. An opening acts on bright objects (areas with the high elevation in LiDAR data, such as the top of the roof) compared with their surrounding, while closings act on dark (low height in the LiDAR data) objects. For example, an opening deletes bright objects that are smaller than the SE[1]. By increasing the size of the SE and repeating the previous operation, a complete morphological profile (MP) is built, carrying information about the size and the shape of objects in the image.

In our experiments, morphological features are generated by applying morphological openings and closings with partial reconstruction [12]–[14] on both LiDAR data and the first 2 principal components (PCs) (representing more than 99% of the cumulative variance) of original HS image. For disk-shaped SE, MPs with 15 openings and closings (ranging from 1 to 15 with step size increment of 1) are computed for both LiDAR data and the first 2 PCs of HS image. For linear structuring elements, we take the maximum (for openings) or minimum (for closings) over multiple orientations (every 10 degrees), and use 10% of the length of the SE for partial reconstruction. Then, we generate MPs with 20 openings and closings (ranging from 5 to 100 with step size increment of 5) for both LiDAR data and the first 2 PCs of HS image. Fig. 1 shows the results of MP with partial reconstruction for LiDAR data with different scales. As the size of the SE increases in openings, we can see that more and more bright objects (i.e. objects with high elevation) disappear in the dark background of LiDAR data. The effect of using disk-based and linear-based morphological features with partial reconstruction for classification of remote sensing data from urban areas has been discussed in our previous work [12]–[14].

[1]Deleting means here that the pixels in the object take on the value of their surrounding

III. Proposed fusion method

Different feature sources typically have different range of values, different dimensions and different characteristics. For example, an original HS image with 144 bands contains the spectral information of the ground covers. The morphological features of LiDAR data with 70 bands (with 30 bands disk-based MP and 40 bands directional MP) carry the elevation information of the same surveyed area. The morphological features obtained from the HS image has 140 bands and carries the spatial information. Before fusing all the feature sources, we normalize their dimensions and reduce the noise throughout the given feature space with Kernel Principal Component Analysis (KPCA) [14], [15], like we also did in [11]. We assume that the dimension of each feature source is already normalized to the smallest dimension of all the feature sources $D = 70$. Let $\mathbf{X}^{Spe} = \{\mathbf{x}_i^{Spe}\}_{i=1}^n$, $\mathbf{X}^{Spa} = \{\mathbf{x}_i^{Spa}\}_{i=1}^n$ and $\mathbf{X}^{Ele} = \{\mathbf{x}_i^{Ele}\}_{i=1}^n$ denote the spectral, spatial (the spatial features are obtained from the hyperspectral data) and elevation features, respectively, where $\mathbf{x}_i^{Spe} \in \mathbb{R}^D$, $\mathbf{x}_i^{Spa} \in \mathbb{R}^D$ and $\mathbf{x}_i^{Ele} \in \mathbb{R}^D$ after normalization to the same dimension. $\mathbf{X}^{Sta} = \{\mathbf{x}_i^{Sta}\}_{i=1}^n = [\mathbf{X}^{Spe}; \mathbf{X}^{Spa}; \mathbf{X}^{Ele}]$, and $\mathbf{x}_i^{Sta} = [\mathbf{x}_i^{Spe}; \mathbf{x}_i^{Spa}; \mathbf{x}_i^{Ele}] \in \mathbb{R}^{3D}$ denotes the vector stacked by the spectral, spatial and altitude features. $\{\mathbf{z}_i\}_{i=1}^n$, and $\mathbf{z}_i \in \mathbb{R}^d$ denote the fusion features in a lower dimensional feature space with $d \leq 3D$.

The goal of this paper is to find a transformation matrix $\mathbf{W} \in \mathbb{R}^{3D \times d}$, which can couple dimensionality reduction and feature fusion in a way of $\mathbf{z}_i = \mathbf{W}^T \mathbf{x}_i$ ($\mathbf{x}_i$ is a variable, which can be set to be $\mathbf{x}_i^{Sta}$, $\mathbf{x}_i^{Spe}$ and etc.). The transformation matrix $\mathbf{W}$ should not only fuse different features in a lower dimensional feature space, but also preserve local neighborhood information and detect the manifold embedded in the high-dimensional feature space. A reasonable way [16] to find the transformation matrix $\mathbf{W}$ can be defined as follows:

$$\arg \min_{\mathbf{W} \in \mathbb{R}^{3D \times d}} \Big(\sum_{i,j=1}^{n} ||\mathbf{W}^T \mathbf{x}_i - \mathbf{W}^T \mathbf{x}_j||^2 A_{ij} \Big) \qquad (1)$$

where the matrix $\mathbf{A}$ is the edge of the graph $\mathbf{G} = (\mathbf{X}, \mathbf{A})$.

In our previous work [11], we assumed that the edges (between data points $\mathbf{x}_i$ and $\mathbf{x}_j$) are binary, i.e. $A_{ij} \in \{0, 1\}$. $A_{ij} = 1$ if $\mathbf{x}_i$ and $\mathbf{x}_j$ are "close" and $A_{ij} = 0$ if $\mathbf{x}_i$ and $\mathbf{x}_j$ are "far apart". The "close" was defined by finding the k nearest neighbors (NN) of the data point $\mathbf{x}_i$. The k NN is determined first by calculating the Euclidean distance between data point $\mathbf{x}_i$ and all the data points, then sorting the distance and determining nearest neighbors based on the k-th minimum distance. A fusion graph $\mathbf{G}^{Fus} = (\mathbf{X}^{Sta}, \mathbf{A}^{Fus})$ was defined as follows:

$$\mathbf{A}^{Fus} = \mathbf{A}^{Spe} \odot \mathbf{A}^{Spa} \odot \mathbf{A}^{Ele} \qquad (2)$$

with '$\odot$' denoting element-wise multiplication, i.e. $A_{i,j}^{Fus} = A_{i,j}^{Spe} A_{i,j}^{Spa} A_{i,j}^{Ele}$, $A_{ij}^{Fus} = 1$ only if $A_{ij}^{Spe} = 1$, $A_{ij}^{Spa} = 1$ and $A_{ij}^{Ele} = 1$. In this definition, all the connected nodes had the same weight on their edges, without accounting for actual differences in the spectral, spatial and elevation proximities of different data point pairs. However, this may not be true in

real cases. For example, it is more probable that a data point has similar characteristics with its nearest neighbors than with those points that are far apart. Therefore, in this paper, we propose a *generalized* fusion graph $\mathbf{G}^{GFus} = (\mathbf{X}^{Sta}, \mathbf{Q}^{GFus})$. Suppose Δ is a pairwise distance matrix of the stacked features $\mathbf{X}^{Sta}$. We propose a fused distance matrix as:

$$\Delta^{GFus} = \Delta + \mathbf{A}^{Neg} \max(\Delta) \tag{3}$$

where $\mathbf{A}^{Neg} = \neg\mathbf{A}^{Fus}$ and the operator '$\neg$' denotes logical negation. Let $\mathcal{N}_i$ denote the k nearest neighbors of $\mathbf{x}_i$. For each node $\mathbf{x}_i$, ($i \in \{1, \cdots, n\}$), we first find its k nearest neighbors $\mathcal{N}_i$ in the fused distance matrix Δ^{GFus}. The edges are then formally defined as:

$$Q_{ij}^{GFus} = \begin{cases} e^{-||\mathbf{x}_i - \mathbf{x}_j||}, & \text{if } \mathbf{x}_j \in \mathcal{N}_i, \\ 0, & \text{otherwise}, \end{cases} \tag{4}$$

Note that the edges denoted by $\mathbf{A}^{Fus}$ or $\mathbf{A}^{Neg}$ are still binary, while the edges of $\mathbf{Q}^{GFus}$ are weighted with different values according to their distance if they are connected. The use of the neighborhood $\mathcal{N}_i$ in this equation guarantees that those data points that differ strongly in any of the spectral, spatial or elevation characteristics will not be connected in the graph. For example, the data points from football fields made of real grass ($\mathbf{x}_i^{Sta}$) and those made of synthetic grass ($\mathbf{x}_j^{Sta}$) have very similar spatial and altitude information ($\mathbf{A}_{i,j}^{Spa} = 1$, $\mathbf{A}_{i,j}^{Ele} = 1$), but different spectral characteristics ($\mathbf{A}_{i,j}^{Spe} = 0$). Then, $A_{i,j}^{Neg} = 1$ and the distance $\Delta_{i,j}^{GFus}$ in (3) will be penalized by adding the maximum value of Δ. Hence the data points that are strongly dissimilar in any of the three characteristics are not likely to be within each other's k nearest neighbors, i.e. they are not likely to be connected in the fused graph. When using the constraint in [17] for avoiding degeneracy:

$$\mathbf{W}^T(\mathbf{X}^{Sta})\mathbf{D}^{GFus}(\mathbf{X}^{Sta})^T\mathbf{W} = \mathbf{I} \tag{5}$$

where $\mathbf{D}^{GFus}$ is a diagonal matrix with $D_{i,i}^{GFus} = \sum_{j=1}^{n} Q_{i,j}^{GFus}$ and $\mathbf{I}$ the identity matrix, we can obtain the transformation matrix $\mathbf{W} = (\mathbf{w}_1, \mathbf{w}_2, \cdots, \mathbf{w}_r)$ which is made up by r eigenvectors associated with the least r eigenvalues $\lambda_1 \leq \lambda_2 \leq \cdots \leq \lambda_r$ of the following generalized eigenvalue problem:

$$(\mathbf{X}^{Sta})\mathbf{L}^{GFus}(\mathbf{X}^{Sta})^T\mathbf{w} = \lambda(\mathbf{X}^{Sta})\mathbf{D}^{GFus}(\mathbf{X}^{Sta})^T\mathbf{w} \tag{6}$$

where $\mathbf{L}^{GFus} = \mathbf{D}^{GFus} - \mathbf{Q}^{GFus}$ is the fusion Laplacian matrix.

IV. Experimental Results

Experiments are done on a hyperspectral image and a LiDAR data which were acquired by the NSF-funded Center for Airborne Laser Mapping (NCALM) on June 2012 over the University of Houston campus and the neighboring urban area. The hyperspectral imagery has 144 spectral bands with wavelength range from 380 nm to 1050 nm. Both datasets have the same spatial resolution (2.5m). The whole scene of the data, consisting of the full 349 $\times$ 1905 pixels, contains 15 classes. Available training and testing set are given in Table I (# number of training samples/ # number of test samples), and Fig. 2 shows false color image of HS data and test samples. For more information, see [18].

The SVM classifier with radial basis function (RBF) [19] kernels is applied in our experiments. The parameters of SVM classifier are set the same as in our previous work [11]. Different feature sources are scaled to $[-1, 1]$ before classification. We compare our proposed GGF with the schemes of (1) Using original HSI; (2) Using the MPs computed on the first 2 PCs of original HSI (MPs$_{HSI}$); (3) Using the MPs computed on the LiDAR data (MPs$_{LiDAR}$); (4) Stacking morphological features computed from both LiDAR data and the first 2 PCs of original HS image (MPs$_{HSLi}$), similarly as [6]; (5) Stacking all dimensional normalized features, i.e. $\mathbf{X}^{Sta}$ (Sta); (6) Stacking all the features extracted by PCA from each individual features which represents more than 99% of the cumulative variance (PCA); (7) Stacking all the features extracted by NWFE [20] from each individual feature (which represents more than 99% of the cumulative variance); (8) Features fused by using the graph constructed by all stacked feature sources (i.e. LPP [17]) (LPP); (9) Our previous work with the edges of the fusion graph binary [11] (GFHL). Both GFHL and our proposed GGF can operate on all feature sources without and with KPCA normalization. We denote feature fusion on original feature sources without KPCA normalization as GFHL$_{org}$ and GGF$_{org}$, respectively. In our experiments, 5000 samples were randomly selected to train KPCA, LPP, GFHL and our proposed GGF.

The classification results are quantitatively evaluated by measuring the Overall Accuracy (OA), the Average Accuracy (AA) and the Kappa coefficient (κ) on the test samples. The experiments were carried out on 64-b, 3.40 GHz Intel i7-4930K (1 core) CPU computer with 64 GB memory, the consumed time includes normalization, feature fusion and classification. Table I shows the accuracies and consumed time obtained from the experiments. For visual comparison, we show the classification maps in Fig. 2.

Form the table and figure, we have the following findings:

1) The results confirm that fusion of the spectral, the spatial and the elevation features can improve the classification performances. In particular, our proposed GGF produced the best OA, AA and κ. The improvements of GGF in OA are 3.50%-12.93% compared to the schemes of (1)-(8). Although increasing the processing time with KPCA normalization, both GFHL and GGF have more than 3% improvements in κ compared to the GFHL$_{org}$ and GGF$_{org}$ without KPCA normalization. Compared to setting the edge of fusion graph binary (GFHL) in [11], the proposed generalized fusion graph (GGF) produces higher overall accuracies, especially without KPCA normalization.
2) From the class-specific accuracies, when single features are used, the Raw$_{HSI}$ approach produces better results on class 'Tree', whereas the MPs$_{HSI}$ performs better on classes 'Residential' and 'Road', and the MPs$_{LiDAR}$ approach performs better on classes 'Commercial' and

TABLE I: Classification accuracies obtained by the described schemes.

	Raw$_{HS}$	MPs$_{HS}$	MPs$_{Li}$	MPs$_{HSLi}$	Sta	PCA	NWFE	LPP	GFHL$_{org}$	GGF$_{org}$	GFHL	GGF
Number of Features	144	140	70	210	210	35	42	26	36	28	24	22
OA (%)	80.72	82.43	69.39	86.39	87.49	85.28	87.96	90.74	88.59	91.28	93.29	**94.0**
AA (%)	83.40	84.99	68.42	88.48	88.94	87.29	88.88	91.26	89.43	91.24	93.19	**93.79**
κ	0.792	0.810	0.668	0.853	0.864	0.840	0.869	0.900	0.876	0.903	0.927	**0.935**
Consumed Time (s)	238.3	230.9	163.9	258.9	1159.4	88.1	1338.2	655.7	131.3	83.4	628.8	629.6
(#198 / #1053) Grass Healthy	82.15	80.25	35.61	82.43	81.10	78.63	81.29	**82.91**	82.72	82.53	82.24	**82.91**
(#190 / #1064) Grass Stressed	81.58	80.64	67.11	82.61	84.87	81.77	83.27	87.41	84.96	98.68	88.91	**99.34**
(#192 / #505) Grass Synthetis	99.80	**100**	79.60	**100**	**100**	**100**	**100**	**100**	**100**	**100**	**100**	**100**
(#188 / #1056) Tree	92.80	84.09	72.92	91.10	95.45	93.75	89.49	98.86	97.73	98.96	99.24	**99.34**
(#186 / #1056) Soil	97.92	**100**	83.52	99.91	99.91	99.91	99.81	99.91	99.15	**100**	**100**	**100**
(#182 / #143) Water	95.10	95.10	66.43	**100**	95.80	95.80	95.80	95.10	95.80	95.10	95.10	95.10
(#196 / #1072) Residential	76.21	87.31	76.59	80.97	86.94	84.70	86.38	**92.28**	87.22	90.95	89.18	90.86
(#191 / #1053) Commercial	54.51	45.58	91.03	63.06	59.54	66.95	76.07	86.23	85.38	90.98	95.54	**95.63**
(#193 / #1059) Road	78.47	91.03	59.21	91.88	90.37	83.66	**93.58**	91.88	89.80	90.46	91.03	89.33
(#191 / #1036) Highway	60.04	60.42	64.86	64.67	65.44	57.53	62.16	72.97	66.89	60.91	**98.65**	92.76
(#181 / #1054) Railway	79.51	87.10	88.24	93.45	**99.24**	97.34	98.39	96.87	98.20	94.46	97.34	96.58
(#192 / #1041) Parking Lot 1	82.90	86.84	70.89	97.89	99.33	91.74	**99.90**	90.2	84.62	99.14	88.95	91.93
(#184 / #285) Parking Lot 2	72.63	76.49	55.09	**79.30**	77.19	77.54	65.26	76.49	69.82	65.26	73.33	74.39
(#181 / #247) Tennis Court	**100**	**100**	**100**	**100**	**100**	**100**	**100**	**100**	**100**	**100**	**100**	**100**
(#187 / #473) Running Track	97.25	**100**	14.80	**100**	98.94	**100**	**100**	98.73	99.15	99.15	98.31	98.73

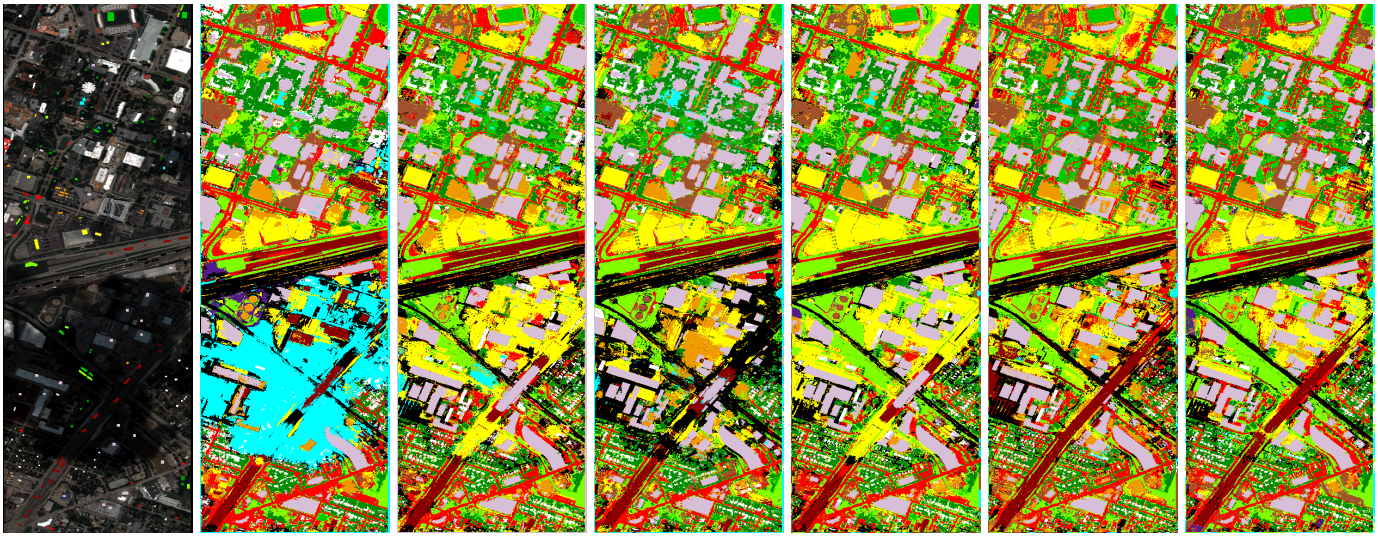

(a) (b) (c) (d) (e) (f) (g)

Fig. 2: Classification maps produced by the described schemes. (a) False color image with 15 classes labeled and highlighted in the image; and thematic maps using (b) MPs$_{HSLi}$; (c) LPP; (d) GFHL$_{Org}$; (e) GGF$_{Org}$; (f) GFHL [11]; (g) GGF.

'Highway'. The proposed GGF produces higher accuracy on some classes related to nature resources, e.g. grass and tree. For some man-made objects such as 'Commercial' and 'Highway', both GFHL and GGF perform better than the schemes of (1)-(8).

3) From the classification maps, we can see visually that the objects under cloud regions are not well classified by using the stacked features. Without KPCA normalization, the proposed GGF$_{org}$ classifies objects under cloud better than GFHL$_{org}$, with less consumed time.

The remote sensing data from urban area was a mix between man-made structures and natural materials, different objects may be made by same materials. It is difficult to classify them only using hyperspectral data, for example, some land use classes (e.g. commercial and highway) are better classified when using LiDAR data. Because commercial objects have larger area and higher elevation than residential objects and highway objects have higher elevation than road objects. By concentrating different features in the stacked structure, the classification accuracies are improved. The approaches of NWFE and Sta are similar to the PCA approach in terms of a stacked architecture, all these three approaches first applied feature extraction on each individual feature, then concatenated the extracted feature vectors from the original HS data, the MPs of HS image and the MPs of LiDAR into one stacked vector. The differences are that each individual feature is represented by different aspects, e.g. the features extracted by PCA represent most of the cumulative variance in the data, while the features extracted by NWFE respect the class discriminant. The cloud-covered regions in original HS image are not classified well by fusing features in a stacked architecture, because the elevation information contained in the morphological features of LiDAR data is not well represented in such a way of data fusion. The spectral and the spatial information (MPs$_{HS}$) of the cloud-covered regions are not related to real ground cover. The LiDAR sensor can penetrate clouds and its morphological features contain the elevation information of the real ground cover. When stacking all feature sources together, the element values of different features can be significantly unbalanced, and the information contained by

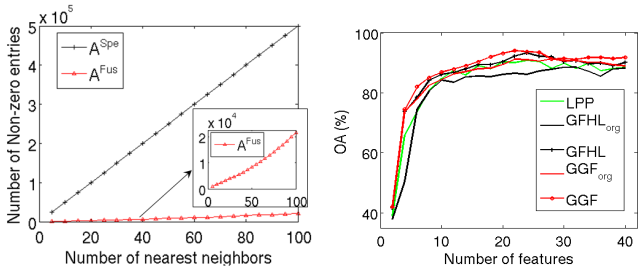

(a) (b)

Fig. 3: (a) The number of non zero entries in $\mathbf{A}^{Spe}$ and $\mathbf{A}^{Fus}$ as a function of the number of the nearest neighbors. (b) The OA on the number of extracted features.

different feature sources is not equally represented. The same problems happen when using the stacked features to build a graph in LPP method. By building binary fusion graph, GFHL [11] cannot classify some objects under cloud well, especially GFHL$_{org}$ without KPCA normalization. This is because both GFHL and GFHL$_{org}$ set all connected edges of fusion graph to the same weight, which means that all connected points are treated as equally similar in terms of their characteristics. The proposed approach (GGF and GGF$_{org}$) assigns different weights to the connected edges according to a distance function and in this way better models the actual similarity of the connected nodes in their characteristics. Fig. 3(a) shows that there are fewer non-zero entries in $\mathbf{A}^{Fus}$ than in $\mathbf{A}^{Spe}$ (the number of non-zero entries is the same as $\mathbf{A}^{Spa}$ and $\mathbf{A}^{Ele}$) as the number of the nearest neighbors increases. With KPCA dimensional normalization, the OA of both GFHL and our proposed GGF are better than those without KPCA normalization (i.e. GFHL$_{org}$ and GGF$_{org}$) as the number of extracted features increases, see Fig. 3(b).

V. CONCLUSION

The main contribution of this paper is a new methodology to include spectral, spatial and elevation information in the classification process by a generalized graph-based feature fusion scheme. Compared to an older related method that used binary edges in the fusion graph, our new method, which employs weighted edges based on differences among spectral, spatial and elevation features, better models the actual similarity of the connected nodes, which is reflected in improved classification performances.

ACKNOWLEDGMENT

The authors would like to thank the Hyperspectral Image Analysis group and the NSF Funded Center for Airborne Laser Mapping (NCALM) at the University of Houston for providing the data sets used in this study, and the IEEE GRSS Data Fusion Technical Committee for organizing the 2013 Data Fusion Contest.

REFERENCES

[1] E. Simental, D. J. Ragsdale, E. Bosch, R. Dodge, Jr., and R. Pazak, "Hyperspectral dimension reduction and elevation data for supervised image classification," *in Proc. 14th ASPRS Conf.*, Anchorage, AK, May 3–9, 2003.

[2] D. Lemp and U. Weidner, "Improvements of roof surface classification using hyperspectral and laser scanning data," *in Proc. ISPRS Joint Conf.: 3rd Int. Symp. Remote Sens. Data Fusion Over Urban Areas (URBAN), 5th Int. Symp. Remote Sens. Urban Areas (URS)*, Tempe, AZ, Mar. 14–16, 2005.

[3] B. Koetz, G. Sun, F. Morsdorf, K. J. Ranson, M. Kneubhler, K. Itten et al., "Fusion of imaging spectrometer and LIDAR data over combined radiative transfer models for forest canopy characterization," *Remote Sensing of Environment*, vol. 106, no. 4, pp. 449–459, 2007.

[4] X. Huang, L. Zhang and W. Gong, "Information fusion of aerial images and LIDAR data in urban areas: vector-stacking, re-classification and post-processing approaches," *International Journal of Remote Sensing* vol. 32, no. 1, pp. 69–84, 2011.

[5] M. Dalponte, L. Bruzzone, D. Gianelle, "Fusion of Hyperspectral and LIDAR Remote Sensing Data for Classification of Complex Forest Areas," *IEEE Trans. Geosci. Remote Sens.*, vol. 46, no. 5, pp. 1416–1427, May 2008.

[6] M. Pedergnana, P. Reddy Marpu, M. Dalla Mura, J. A. Benediktsson, L. Bruzzone, "Classification of Remote Sensing Optical and LiDAR Data Using Extended Attribute Profiles," *IEEE Journals on Selected Topics in Signal Processing*, vol. 6, no. 7, pp. 856–865, Nov. 2012.

[7] L. Zhang, L. Zhang, D. Tao and X. Huang, "On Combining Multiple Features for Hyperspectral Remote Sensing Image Classification," *IEEE Trans. Geosci. Remote Sens.*, vol. 50, no. 3, pp. 879–893 , March 2012.

[8] X. Huang and L. Zhang, "An SVM Ensemble Approach Combining Spectral, Structural, and Semantic Features for the Classification of High-Resolution Remotely Sensed Imagery," *IEEE Trans. Geosci. Remote Sens.*, vol. 51, no. 1, pp. 257–272, Jan. 2013.

[9] M. Dalla Mura, J. A. Benediktsson, B. Waske, and L. Bruzzone, "Extended profiles with morphological attribute filters for the analysis of hyperspectral data," *Int. J. Remote Sens.*, vol. 31, no. 22, pp. 5975-5991, Nov. 2010.

[10] M. Dalla Mura, A. Villa, J. A. Benediktsson, J. Chanussot, L. Bruzzone, "Classification of Hyperspectral Images by Using Extended Morphological Attribute Profiles and Independent Component Analysis," *IEEE Geosci. Remote Sens. Lett.*, Vol. 8, No. 3, pp. 541-545, May 2011.

[11] C. Debes, A. Merentitis, R. Heremans, J. Hahn, N. Frangiadakis, T. Kasteren, W. Liao, R. Bellens, A. Pizurica, S. Gautama, W. Philips, S. Prasad, Q. Du, F. Pacifici, "Hyperspectral and LiDAR Data Fusion: Outcome of the 2013 GRSS Data Fusion Contest," *IEEE Journal of Selected Topics in Applied Earth Observations and Remote Sensing*, 2014 (In Press).

[12] W. Liao, R. Bellens, A. Pižurica, W. Philips and Y. Pi, "Classification of Hyperspectral Data Over Urban Areas Using Directional Morphological Profiles and Semi-Supervised Feature Extraction," *IEEE Journal of Selected Topics in Applied Earth Observations and Remote Sensing*, vol. 5, no. 4, pp. 1177–1190, Aug. 2012.

[13] R. Bellens, S. Gautama, L. Martinez-Fonte, W. Philips, J.C.-W. Chan, F. Canters, "Improved classification of VHR images of urban areas using directional morphological profiles", *IEEE Trans. Geosci. Remote Sens.*, vol. 46, no. 10, pp. 2803–2812, Oct. 2008.

[14] W. Liao, R. Bellens, A. Pižurica, W. Philips, Y. Pi, "Classification of Hyperspectral Data over Urban Areas based on Extended Morphological Profile with Partial Reconstruction", *In Proc. Advanced Concepts for Intelligent Vision Systems (ACIVS) 2012*, Brno, Czech Republic, pp. 278–289, 2012.

[15] B. Scholkopf, A.J. Smola and K.R. Muller, "Nonlinear component analysis as a kernel eigenvalue problem," *Neural Computation*, vol. 10, pp. 1299–1319, 1998.

[16] M. Belkin and P. Niyogi, "Laplacian Eigenmaps and Spectral Techniques for Embedding and Clustering," *Advances in Neural Information Processing Systems 14*, pp. 585–591, MIT Press, 2001.

[17] X. F. He, P. Niyogi, "Locality preserving projections," *Advances in Neural Information Processing Systems 16*, pp. 153-160, MIT Press, Cambridge, 2004.

[18] 2013 IEEE GRSS Data Fusion Contest, Online: *http://www.grss-ieee.org/community/technical-committees/data-fusion/.*

[19] C. C. Chang and C. J. Lin, "LIBSVM: A Library for Support Vector Machines", 2001, *http://www.csie.ntu.edu.tw/ ˜cjlin/libsvm.*

[20] B. C. Kuo and D. A. Landgrebe, "Nonparametric weighted feature extraction for classification", *IEEE Trans. Geosci. Remote Sens.*, vol. 42, no. 5, pp. 1096–1105, May 2004.

[21] M. Fauvel, J. A. Benediktsson, J. Chanussot and J. R. Sveinsson, "Spectral and Spatial Classification of Hyperspectral Data Using SVMs and Morphological Profile", *IEEE Trans. Geosci. Remote Sens.*, vol. 46, no. 11, pp. 3804-3814, Nov. 2008.